RESEARCH ARTICLE

Muscle-Inspired Anisotropic Hydrogels via Pre-Stretching for Direction-Sensitive Human Motion Monitoring

Lixin Zhang[1], Zixuan Yang[1], Weihua Luo[1], Ruiqi Zhao[1], Xushuai Chen[1], Hongming Lu[1], Xi Chen[1,*] and Luke Yan[1,*]

[1] Polymer Materials & Engineering Department, School of Materials Science & Engineering, Chang'an University, Xi'an 710064, China

Abstract

Traditional hydrogels often exhibit disordered molecular structures, resulting in limited mechanical strength, toughness, and functionality, which restrict their practical applications. Here, we engineer an anisotropic Zr^{4+}-crosslinked P(DMA-AA)-CMC hydrogel via pre-stretching to mimic muscle-like alignment. This strategy enhances mechanical strength (5.6 MPa along orientation axis, $1.8\times$ higher than perpendicular) and directional sensitivity through Zr^{4+}-stabilized microstructural ordering. The sensor achieves 303% $\Delta R/R_0$ at 100% strain with $2.2\times$ higher sensitivity parallel to pre-stretch direction, enabling precise movement/orientation tracking. It maintains stability over 200 cycles and accurately monitors joint kinematics (e.g., elbow/knee flexion). This biomimetic design advances wearable sensors for human-machine interfaces.

Keywords: anisotropic hydrogel, directional sensing, wearable sensors, human-machine interfaces.

1 Introduction

Hydrogel-based sensors have emerged as promising materials for applications in biomedicine, environmental monitoring, wearable devices, and flexible electronics due to their softness, biocompatibility, and tunable conductive properties [1–6]. Critical performance metrics such as detection limit, sensing range, response time, and sensitivity directly determine their practical utility. High sensitivity, in particular, is essential for precise detection of subtle physiological or environmental changes. This enables advancements in medical diagnostics and real-time health monitoring. Despite progress, achieving consistently high sensitivity in hydrogels remains challenging due to their inherently disordered and isotropic network structures, which limit mechanical strength and electrical responsiveness [7–10]. Biological soft tissues (e.g., muscles [11, 12], cartilage [13–15], ligaments [16–18], and tendons [19–21]) exhibit

Submitted: 12 November 2025
Accepted: 17 December 2025
Published: 22 December 2025

Vol. 1, **No.** 1, 2025.
10.62762/JAMR.2025.941906

***Corresponding authors:**
✉ Xi Chen
xi_chen@chd.edu.cn
✉ Luke Yan
yanlk_79@hotmail.com

Citation
Zhang, L., Yang, Z., Luo, W., Zhao, R., Chen, X., Lu, H., Chen, X., & Yan, L. (2025). Muscle-Inspired Anisotropic Hydrogels via Pre-Stretching for Direction-Sensitive Human Motion Monitoring. *Journal of Advanced Materials Research*, 1(1), 18–36.

© 2025 by the Authors. Published by Institute of Central Computation and Knowledge. This is an open access article under the CC BY license (https://creativecommons.org/licenses/by/4.0/).

highly ordered, anisotropic microstructures that optimize mechanical and functional properties. Inspired by this, engineering anisotropic structures in hydrogels has become a key strategy to enhance their sensing capabilities. Pre-stretching, in particular, offers a simple and controllable method to align polymer chains, reduce ion migration resistance, and improve electrical conductivity [22, 23]. For instance, Lin et al. [24] developed a poly(vinyl alcohol)/poly(acrylic acid)/Fe^{3+} hydrogel via mechanical stretching and drying, achieving exceptional tensile stress (47.26 MPa) and conductivity (292.64 mS/m). Similarly, Ghosh et al. [25] fabricated an anisotropic poly(acrylamide-maleic acid-acrylate) hydrogel mimicking unidirectionally oriented muscle fibers, demonstrating high tensile strength (7 MPa), flexibility (370% fracture strain), toughness (16 MJ/m^3), and strain-sensitive conductivity. These studies confirm the viability of microstructure alignment for enhancing sensor performance. However, achieving a balance between mechanical strength and sensitivity in hydrogel sensors remains a challenge.

Here, we propose a pre-stretching strategy combined with Zr^{4+} ion crosslinking to fabricate an anisotropic Zr^{4+}-crosslinked poly (N,N-dimethylacrylamide-acrylic acid-carboxymethyl cellulose) (Zr^{4+}-P(DMAA-AA)-CMC) hydrogel. This design synergistically enhances mechanical strength, electrical conductivity, and strain sensitivity while ensuring stability under dynamic conditions. The structure and performance were comprehensively characterized using SEM, POM, FTIR, XPS, and TGA. Its exceptional strain-sensing capabilities enable real-time monitoring of human motions, highlighting potential applications in wearable health monitoring and flexible electronics.

2 Experimental Section

2.1 Materials

N,N-Dimethylacrylamide (DMAA) and carboxymethyl cellulose (CMC) were purchased from Shanghai Easyborn Chemical Technology Co., Ltd. Acrylic acid (AA), N,N′-methylenebisacrylamide (MBAA), and zirconyl chloride octahydrate ($ZrOCl_2{\cdot}8H_2O$) were obtained from Shanghai Aladdin Biochemical Technology Co., Ltd. The azo-based initiator (AIBA) was sourced from Shanghai Yuanye Bio-Technology Co., Ltd. Deionized (DI) water was used throughout all experiments.

2.2 Synthesis of P(DMAA-AA) Hydrogel

A solution of 4.32 g acrylic acid (AA) in 30 mL DI water was prepared under stirring until complete dissolution. Then, 3.96 g N,N-dimethylacrylamide (DMAA) was added and homogenized using a glass rod. Subsequently, 0.03 g of chemical crosslinker N,N′-methylenebisacrylamide (MBAA) and photoinitiator AIBA were introduced into the mixture with continuous stirring. The solution was transferred into a mold via pipette and exposed to UV light (wavelength: 365 nm) for 3 min to yield the P(DMAA-AA) hydrogel.

2.3 Synthesis of P(DMAA-AA)-CMC Hydrogel

First, 1 g CMC powder was dispersed in 20 mL hot water (70°C) and stirred for 20 min using a magnetic stirrer to ensure complete dissolution. The solution was then sonicated for 20 min to eliminate bubbles. Separately, 4.32 g AA and 3.96 g DMAA were dissolved in 30 mL DI water. Then, 4.2 g of the prepared CMC solution was incorporated into the monomer mixture. After each addition, the solution was stirred and sonicated to achieve homogeneity and remove air bubbles. Next, 0.03 g MBAA and AIBA were added under stirring. The mixture was transferred into a mold and UV-irradiated for 3 min to obtain the crosslinked P(DMAA-AA)-CMC hydrogel.

2.4 Preparation of Zr^{4+}-P(DMAA-AA)-CMC Hydrogel

The P(DMAA-AA)-CMC hydrogel was immersed in 500 mL of 0.5 M $ZrOCl_2{\cdot}8H_2O$ solution for 24 h to facilitate Zr^{4+} coordination. The hydrogel was then thoroughly rinsed with DI water to remove unbound Zr^{4+} ions, yielding the Zr^{4+}-crosslinked P(DMAA-AA)-CMC hydrogel.

2.5 Fabrication of Pre-stretched Zr^{4+}-P(DMAA-AA)-CMC Hydrogel

The oriented hydrogels were fabricated using a custom-made stretching mold. First, P(DMAA-AA)-CMC hydrogel was cut into rectangular strips (10 mm in width, 40 mm in length, and 2 mm in thickness). Each sample was then clamped and uniaxially stretched to predetermined tensile strains (50%, 100%, 125%, 150%, 175%, or 200%) at constant rates of 25% per minute. Upon reaching the target strain, the sample was immediately secured in the mold to maintain its stretched state. The fixed sample was immersed in 500 mL of 0.5 M $ZrOCl_2{\cdot}8H_2O$ aqueous solution at room temperature for 24 hours to allow ion

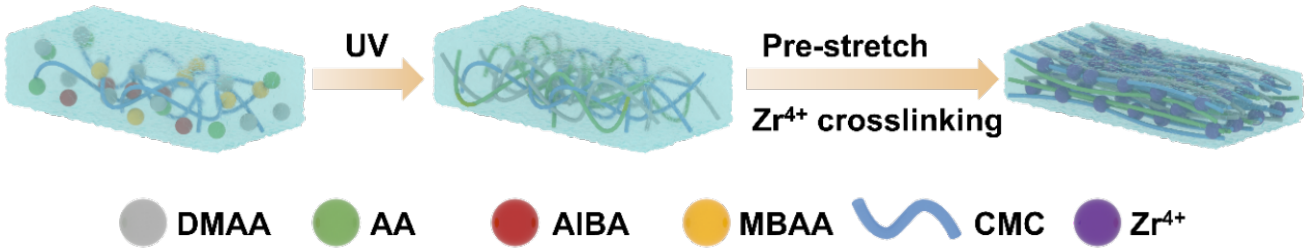


Figure 1. Schematic of the preparation of oriented Zr^{4+}-P(DMAA-AA)-CMC hydrogel.

diffusion and coordination, thereby permanently locking the oriented microstructure formed during pre-stretching. After coordination, the sample was carefully released from the mold and thoroughly rinsed with deionized water to remove unbound ions, yielding the Zr^{4+}-crosslinked oriented hydrogels, denoted as zgel-X% (where X represents the pre-strain percentage, e.g., zgel-125% for 125% pre-strain). This procedure ensures that the alignment induced by mechanical stretching is effectively preserved and stabilized through subsequent ionic crosslinking.

3 Results and Discussion

3.1 Hydrogel Synthesis and Structural Characterization

The fabrication process of oriented Zr^{4+}-crosslinked P(DMAA-AA)-CMC hydrogels is illustrated in Figure 1. Initially, CMC was dissolved in deionized water at 70°C to form a homogeneous transparent solution. Acrylic acid (AA), N, N-dimethylacrylamide (DMAA), and crosslinker N, N'-Methylenebisacrylamide (MBAA) were then polymerized via free-radical polymerization under UV initiation (AIBA) to form P(DMAA-AA)-CMC hydrogels. Hydrogen bonding between CMC and polymer chains enhanced mechanical robustness. The hydrogels were pre-stretched (Parallel to the orientation direction ∥, Perpendicular to the orientation direction ⊥) to varying strains (0–200%) and immobilized using a custom mold. Subsequent immersion in Zr^{4+} solution ($ZrOCl_2 \cdot 8H_2O$) facilitated coordination between Zr^{4+} ions and carboxyl groups ($-COO^-$) of CMC and PAA, yielding oriented zgel-X% hydrogels (where X denotes pre-strain percentage, e.g., zgel-50% for 50% pre-strain). The synergistic combination of pre-stretching and Zr^{4+} cross-linking successfully constructs and stabilizes the anisotropic microstructure of the hydrogel. While the pre-strain is maintained, immersion of the hydrogel into the Zr^{4+} solution enables rapid diffusion of Zr^{4+} ions into the network, where they strongly coordinate with the abundant $-COO^-$ groups on both the CMC and PAA chains. Acting as multidentate cross-linking junctions, the Zr^{4+} ions preferentially bind to the $-COO^-$ groups that are spatially closer and more orderly aligned due to the pre-stretching, thereby forming rigid and stable ionic coordination bonds along the orientation direction. These coordination bonds function as solidified anchoring points, which effectively resist the entropic elastic recoil of the polymer chains after the external force is released, thus "locking" the transient alignment induced by pre-stretching into a permanent, ordered microstructure. All hydrogels (Figure A1) were semi-transparent, colorless, elastic, and exhibiting no macroscopic difference.

Scanning electron microscopy (SEM) revealed porous microstructures in P(DMAA-AA), P(DMAA-AA)-CMC, and Zr^{4+}-P(DMAA-AA)-CMC hydrogels (Figure 2(a-c)). P(DMAA-AA) hydrogels displayed irregular pores with diameters concentrated at 15–20 μm (average: 17.87 μm) (Figure 2(a, d)) [26, 27]. Further introduction of Zr^{4+} ions drastically reduced the average pore size to 5.36 μm with a narrower distribution (Figure 2(c, f)), confirming that Zr^{4+}–carboxyl coordination complexes compacted the polymer network and increased crosslinking density [28]. EDS mapping (Figure A2) confirmed homogeneous distribution of Zr elements post-crosslinking, alongside consistent C, N, and O signals, verifying successful integration of Zr^{4+} without altering bulk composition.

FTIR spectra (Figure 2(g)) displayed characteristic peaks for all hydrogels. P(DMAA-AA) showed broad peaks at 3200–3500 cm^{-1} (O–H/N–H stretching) and 1712 cm^{-1} (C=O stretching). Introducing CMC induced slight shifts in C=O peaks and emerging C–O–C vibrations (1000–1200 cm^{-1}), confirming hydrogen bonding between CMC and polymer chains. For Zr^{4+}-P(DMAA-AA)-CMC, the C=O peak

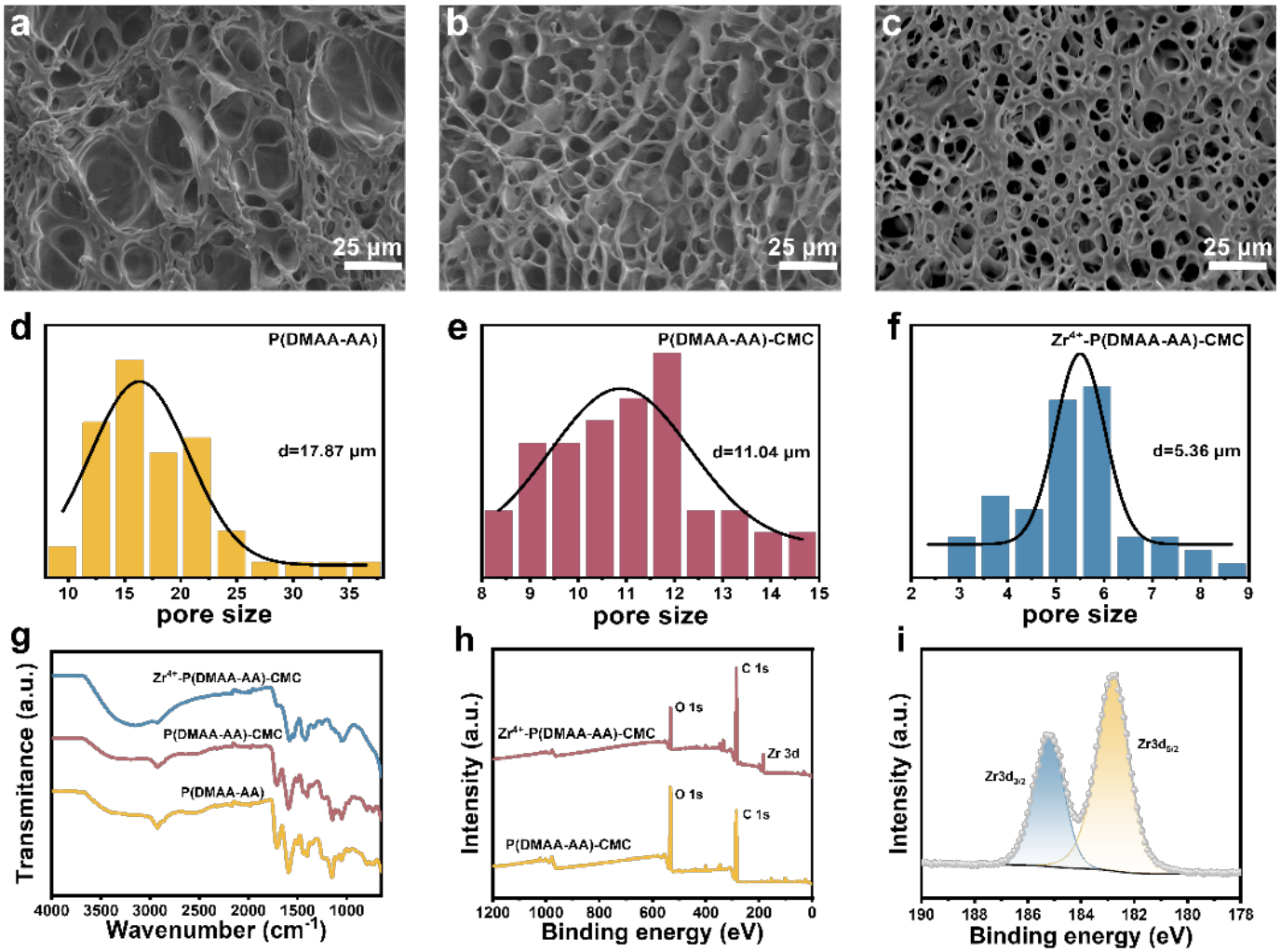


Figure 2. (a–c) SEM images of P(DMAA-AA), P(DMAA-AA)-CMC, and Zr^{4+}-P(DMAA-AA)-CMC hydrogels; (d–f) pore size distribution statistics (calculated using Nanomeasurer software); (g) FTIR spectra; (h) XPS broad-scan spectra of P(DMAA-AA)-CMC and Zr^{4+}-P(DMAA-AA)-CMC hydrogels; (i) Zr 3d high-resolution spectrum of Zr^{4+}-P(DMAA-AA)-CMC hydrogel.

shifted significantly, and new vibrations appeared at 600–800 cm^{-1} (Zr–O stretching), indicating coordination between Zr^{4+} and carboxyl groups. XPS wide-scan spectra (Figure 2(h)) confirmed the presence of Zr elements in Zr^{4+}-crosslinked hydrogels, with distinct Zr 3d peaks at 182.5 eV (Zr $3d_{5/2}$) and 184.9 eV (Zr $3d_{3/2}$) (Figure 2(i)), aligning with Zr^{4+}–carboxyl coordination. Peak deconvolution of O 1s spectra increased $-COO^-/Zr^{4+}$ contributions post-crosslinking, further validating metal-ion coordination.

The properties of the hydrogels were systematically tuned through compositional modification and physical processing, as detailed in the supplementary figures. Figure A3 demonstrates a tunable swelling capacity, where P(DMAA-AA) exhibits the highest equilibrium swelling ratio (117.7 g/g) due to its porous structure, while subsequent incorporation of CMC and Zr^{4+} cross-linking progressively reduces swelling by densifying the network. This increased crosslinking density concurrently enhanced surface hydrophobicity, evidenced by a systematic rise in the contact angle from 21.5° to over 52° (Figure A4). The mechanical properties were significantly reinforced by ionic crosslinking, with the Zr^{4+}-crosslinked hydrogel showing a ∼20-fold increase in tensile stress and a ∼25-fold increase in elastic modulus (Figure A5). Furthermore, the mechanical enhancement was dependent on Zr^{4+} concentration, peaking at 0.5 M before declining at higher concentrations due to over-crosslinking (Figure A6). Subsequent physical modification via pre-stretching induced only physical alignment without chemical change, as confirmed by FTIR (Figure A7). This process further induced microstructural densification, leading to reduced

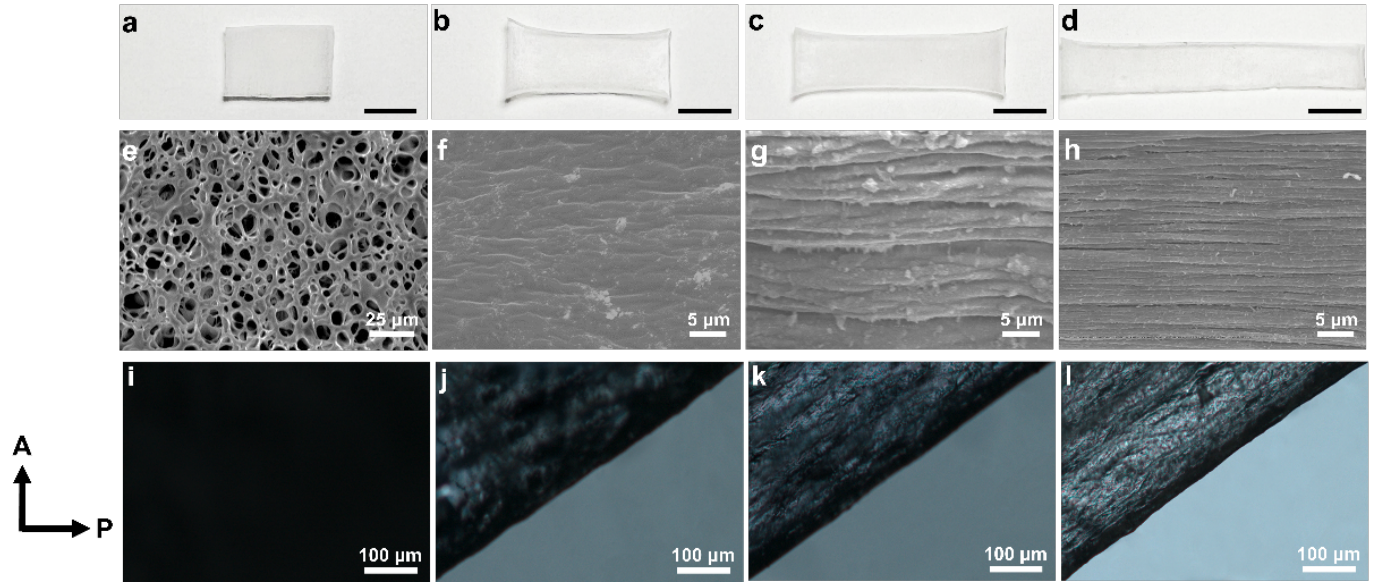


Figure 3. Photographs (a–d) of zgel-X% (X = 0, 50, 100, 200) hydrogels; cross-sectional SEM images (e–h); POM images (i–l).

swelling, lower water content, and enhanced surface hydrophobicity, as summarized in Figure A8.

3.2 Anisotropy and Mechanical Enhancement

To elucidate the microstructural evolution of oriented hydrogels, we systematically analyzed samples subjected to varying pre-strain levels (denoted as zgel-X%, where X represents pre-strain percentage). Macroscopic images (Figure 3 (a–d)) revealed progressive axial elongation with increasing pre-strain, visually confirming alignment along the stretching direction. Scanning electron microscopy (SEM) further demonstrated structural transformations: isotropic P(DMAA-AA)-CMC hydrogels exhibited uniformly distributed porous networks (Figure 3 (e)), whereas pre-stretched samples (Figure 3 (f–h)) displayed reduced porosity and distinct striated patterns parallel to the alignment axis. These patterns intensified at higher pre-strain (e.g., zgel-200%), indicating enhanced polymer chain orientation.

Polarized optical microscopy (POM) provided additional evidence of anisotropy. Unstrained hydrogels showed complete darkness under cross-polarizers (Figure 3 (i)), confirming isotropic behavior. In contrast, pre-stretched samples exhibited pronounced birefringence, with brightness escalating alongside pre-strain (Figure 3 (j-l)). This optical anisotropy aligns with SEM observations, underscoring the role of pre-stretching in inducing microstructural alignment.

Tensile tests along the orientation direction (Figure 4 (a–c)) demonstrated significant mechanical improvements with increasing pre-strain. The zgel-0% ∥ hydrogen exhibited a tensile strength of 1.2 MPa and fracture strain of 101%, while zgel-200% ∥ achieved 5.6 MPa and 204%—representing a 3.7-fold increase in strength and 2.4-fold rise in elastic modulus. This enhancement stems from pre-stretch-induced reorganization of polymer chains into aligned configurations, enabling efficient load distribution [29].

Perpendicular to the orientation (Figure 4 (d–f)), mechanical properties also improved but to a lesser extent. For instance, zgel-200% ⊥ reached 3.0 MPa strength and 168% strain—values notably lower than those along the alignment axis. Comparative analysis (Figure 4 (g–i)) revealed anisotropic ratios of 1.7 (strength), 1.2 (modulus), and 1.3 (strain) for zgel-200%, highlighting the critical influence of chain orientation on mechanical asymmetry.

Oscillatory shear tests confirmed dominant elastic behavior across all pre-strain levels, with storage modulus (G') consistently exceeding loss modulus (G'') (Figure A9). No significant variations in complex viscosity (η) were observed, indicating stable viscoelastic properties despite structural changes.

Tear tests further underscored anisotropy (Figure A10). Isotropic zgel-0% hydrogels displayed similar fracture energy in all directions, whereas zgel-200% exhibited divergent behaviors: zgel-200%∥ tear energy was 65 J m^{-2} (crack propagation along aligned chains via dynamic Zr^{4+} bond dissociation) but zgel-200%⊥ tear

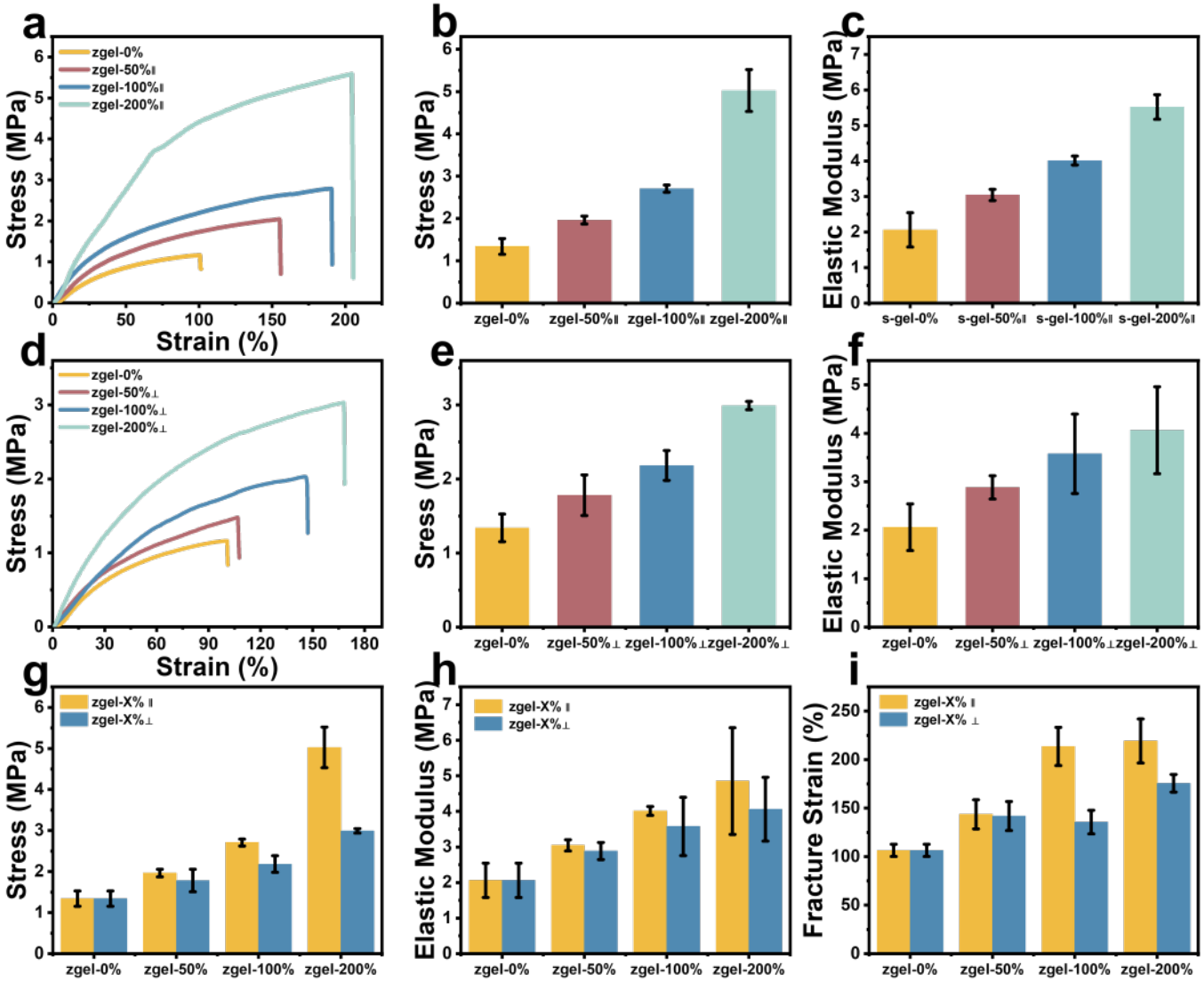


Figure 4. (a) Stress-strain curve, (b) stress plot, and (c) elastic modulus plot of zgel-X% ∥ hydrogel; (d) stress-strain curve, (e) stress plot, and (f) elastic modulus plot of zgel-X% ⊥ hydrogel; Comparison of stress plots (g), elastic modulus plots (h), and strain plots (i) for zgel-X% hydrogels with different orientations.

energy surged to 389 J m^{-2} (crack deflection requiring covalent chain rupture). This 6-fold anisotropy aligns with observations in biomimetic hydrogels designed for tendon/ligament applications.

The synergy between pre-stretching and Zr^{4+} crosslinking drives microstructural alignment and mechanical augmentation. Pre-straining extends random polymer chains into oriented configurations, while Zr^{4+} ions immobilize this structure through coordination with carboxyl groups ($-COO^-$) from CMC and P(AA). This dual mechanism not only enhances tensile properties but also enables strain-dependent conductive pathways for sensing applications [25].

3.3 Electrical Properties and Sensing Performance

The incorporation of Zr^{4+} ions induce coordination crosslinking with carboxylate groups in the hydrogel network, enhancing both mechanical robustness and electrical conductivity by facilitating ion transport pathways [30]. Conductivity directly influences strain sensitivity, as higher conductivity enables pronounced resistance changes ($\Delta R/R_0$) under deformation, critical for high-performance sensing.

To evaluate sensing performance, hydrogels were subjected to uniaxial stretching using a universal testing machine, while real-time resistance changes were recorded via an electrochemical workstation. Figure 5 (a) depicts the $\Delta R/R_0$ versus strain curve for

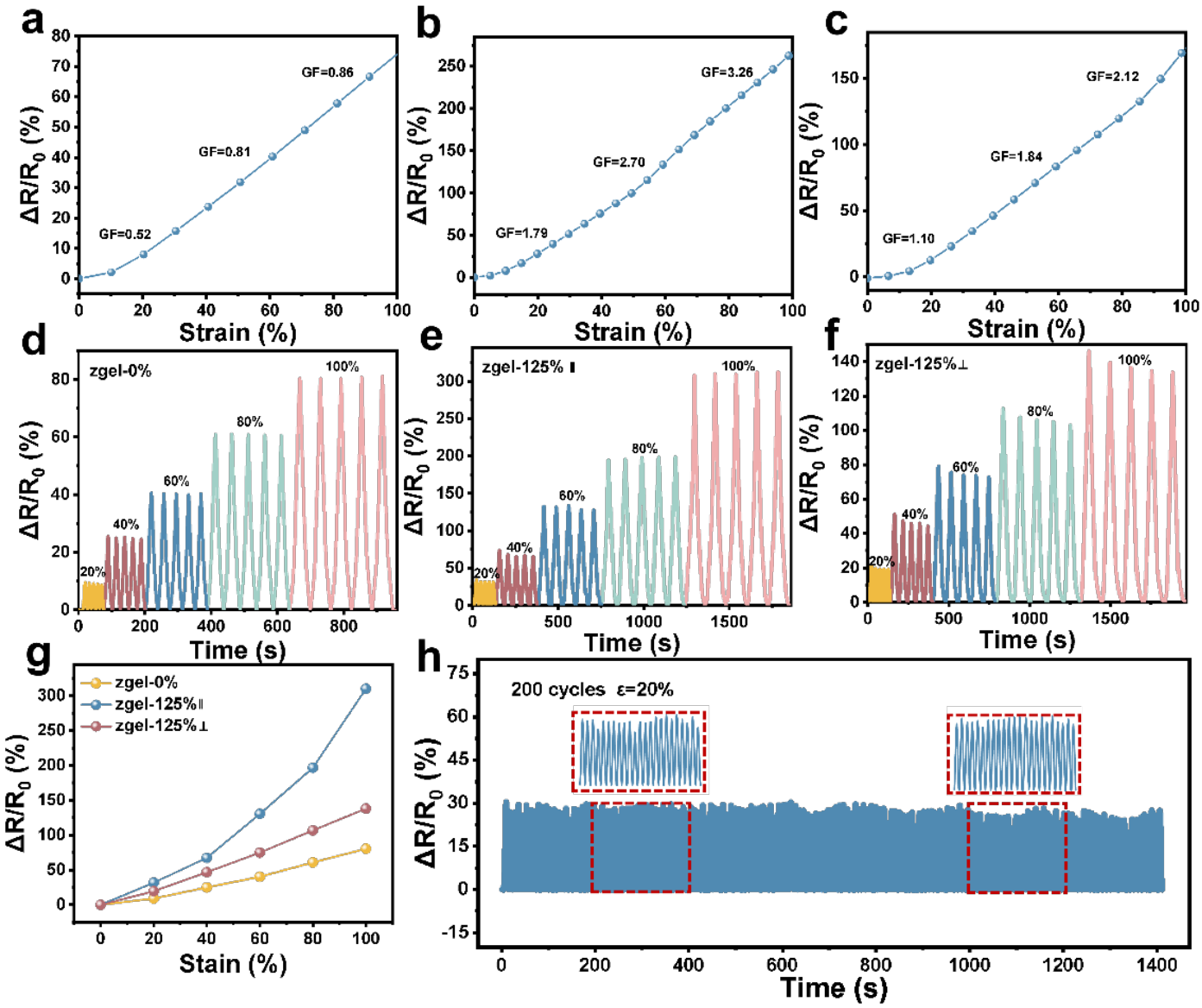


Figure 5. Strain sensors made of zgel-0% hydrogel and zgel-125% (∥ and ⊥) hydrogel: (a–c) Variation of relative resistance with strain; (d–f) Relative resistance changes under different strains; (g) Comparison of relative resistance changes; (h) Cyclic stability of zgel-125% ⊥ hydrogel strain sensor after 200 cycles at 20% tensile strain.

isotropic hydrogels (zgel-0%). The gauge factor (GF), calculated as the slope of this curve, quantifies strain sensitivity. Segmented linear regression revealed GF values of 0.52 (0–30% strain), 0.81 (30–60%), and 0.86 (60–100%), indicating enhanced sensitivity at higher strains due to progressive disruption of conductive pathways [31].

Pre-stretched hydrogels (zgel-125%) exhibited significantly improved sensitivity (Figure 5 (b–c)). GF values reached 1.79 (0–30%), 2.70 (30–60%), and 3.26 (60–100%)—3.1–3.8 times higher than isotropic samples. This enhancement arises from aligned polymer chains reducing ion migration resistance and promoting efficient electron/ion transport. Perpendicular to the orientation, GF values remained lower (1.10, 1.84, and 2.12 for respective strain ranges) yet superior to zgel-0%, confirming that pre-straining universally improves sensitivity regardless of direction [32].

Cyclic stretching tests (20–100% strain, 5 cycles) demonstrated exceptional reproducibility and stability (Figure 5 (d–f)). The zgel-125% ∥ achieved $\Delta R/R_0$ of 310.1% at 100% strain—3.8 times higher than zgel-0% (80.5%)—while zgel-125% ⊥ achieved 138.7% (Figure 5 (g)). All samples maintained consistent $\Delta R/R_0$ across cycles, highlighting structural reversibility. Long-term durability was confirmed via 200 cycles at 20% strain (Figure 5 (h)),

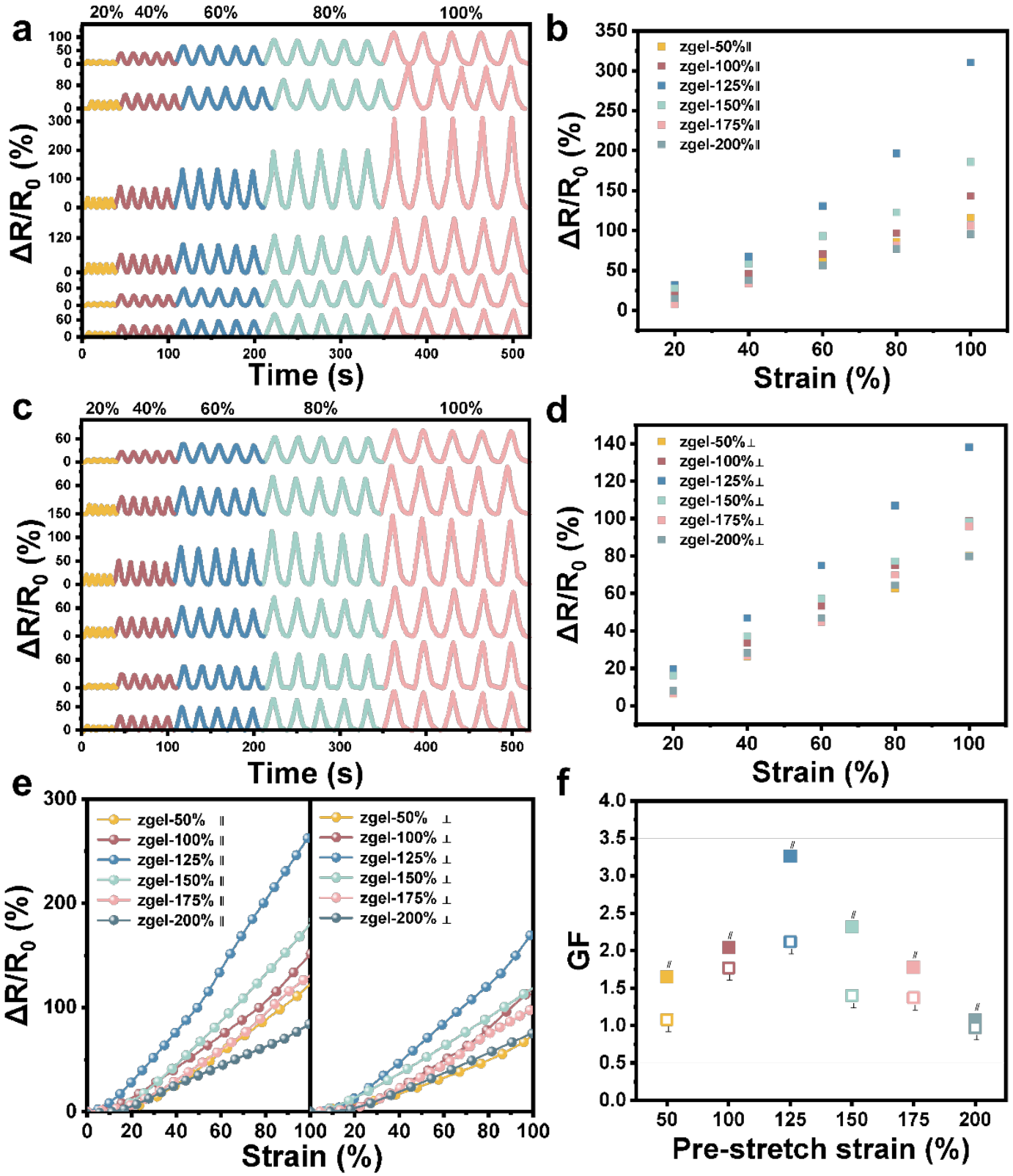


Figure 6. (a) Change in relative resistance of zgel-X% ∥ (X = 50, 100, 125, 150, 175, 200) under different pre-stretch strains; (b) Comparison of relative resistance changes in zgel-X% ∥ under different tensile strains; (c) Relative resistance changes in zgel-X% ⊥ (X = 50, 100, 125, 150, 175, 200) under different pre-stretch strains; (d) Comparison of relative resistance changes in zgel-X% ⊥ under different tensile strains; (e) Comparison of the relationship between relative resistance and strain for strain sensors made from zgel-X% (X = 50, 100, 125, 150, 175, 200); (f) Comparison of GF values for zgel-X% hydrogels oriented parallel and perpendicular to the direction.

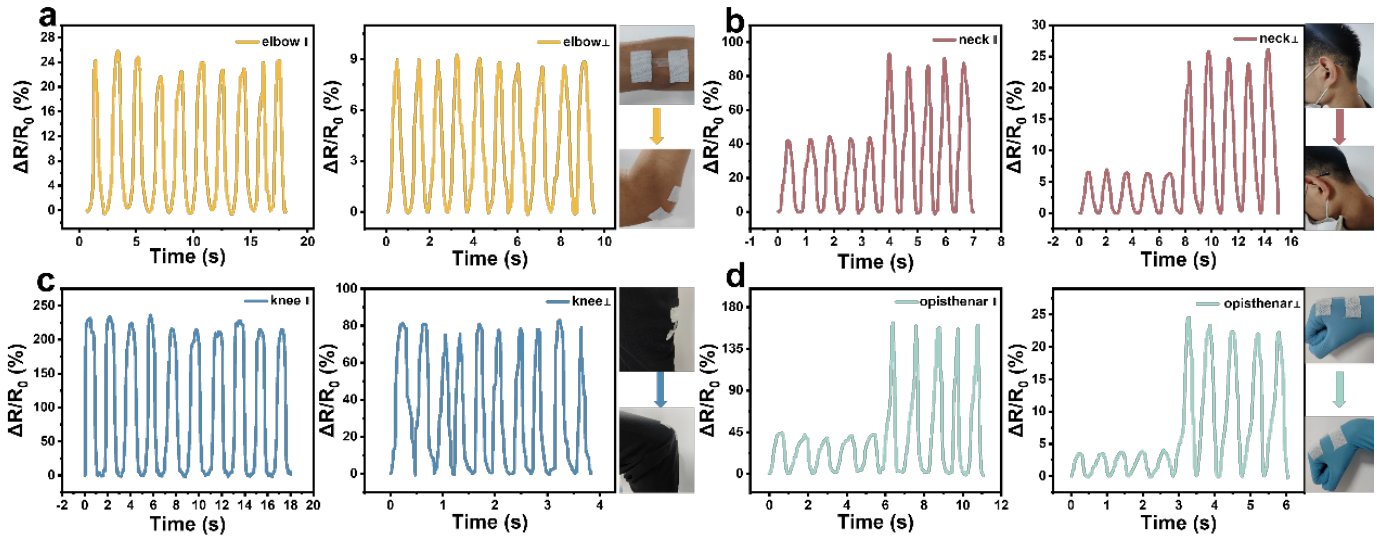


Figure 7. Anisotropic zgel-125% (∥ and ⊥) hydrogel sensors with photographic illustrations for monitoring (a) elbow flexion, (b) neck flexion, (c) knee flexion, and (d) hand dorsiflexion.

where $\Delta R/R_0$ stabilized at ∼30% without signal decay [43].

Pre-strain optimization studies (50–200% pre-strain) revealed zgel-125% as the optimal condition, achieving a gauge factor (GF) of 3.26 within the 60–100% strain range (Figure 6). Beyond 125% pre-strain, the GF declined sharply (e.g., to 1.23 at 150% pre-strain), which is attributed to excessive water loss and microstructural damage that impair the continuity of the conductive ion channels. Detailed relative resistance versus strain curves for all pre-strain levels in both parallel and perpendicular orientations are provided in Figures A11 and A12, further confirming the optimal performance at 125% pre-strain and the consistent directional sensitivity anisotropy across the full range of tested conditions. Anisotropy was consistently observed across all pre-strain levels: the parallel orientation yielded GF values 1.2–1.7 times higher than the perpendicular orientation (Figure 6 (f)), with a maximum anisotropy ratio (sensitivity ratio) of approximately 2.2, underscoring the role of aligned polymer chains and ion pathways in enhancing sensitivity along the stretching axis [33–36]. When contextualized among state-of-the-art anisotropic sensing systems, this anisotropy ratio, while not the highest in absolute terms [37–39], remains significant (see Table A1). It is achieved here through a relatively straightforward and controllable fabrication process combining pre-stretching and ionic crosslinking, offering a favorable balance between performance and manufacturability. Regarding its suitability for complex motion detection, a 2.2-fold directional sensitivity provides a clear signal contrast for distinguishing uniaxial tensile movements along predefined axes, which is sufficient for monitoring basic joint motions or directional deformations.

3.4 Human Motion Monitoring Applications

The anisotropic zgel-125% hydrogel sensor demonstrated robust performance in monitoring joint movements (elbow, knee, hand, neck). zgel-125% ∥ yielded $\Delta R/R_0$ of 24% (elbow bend) and 221% (knee bend)—2.7–2.8 times higher than zgel-125% ⊥ (9% and 79%, respectively) (Figure 7 (a–d)). In practical applications, this design significantly reduces interference from other directions. Resistance changes scaled with motion amplitude and remained stable during cyclic tests, confirming reliability for wearable health monitoring.

4 Conclusion

This study demonstrates the successful fabrication of an anisotropic Zr^{4+}-crosslinked P(DMAA-AA)-CMC hydrogel via pre-stretching and ion coordination. The optimized zgel-125% hydrogel exhibited exceptional mechanical anisotropy (tensile strength: 5.6 MPa, 1.8× higher parallel vs. perpendicular to orientation) and strain-sensitive conductivity, achieving a gauge factor of 3.26 (60–100% strain) with 2.2× higher sensitivity along the alignment axis. The incorporation of CMC and Zr^{4+} enhanced crosslinking density, reducing swelling ratios and improving hydrophobicity for broader environmental adaptability. The sensor maintained stable resistance responses over 200 cycles and detected human joint movements with high

precision ($\Delta R/R_0 = 310.1\%$ at 100% strain). These properties underscore its potential for wearable health monitoring and soft robotics.

Data Availability Statement

Data will be made available on request.

Funding

This work was supported in part by the Innovation Capability Support Program of Shaanxi under Grant 2023-CX-TD-43; in part by the Key Research and Development Program of Shaanxi under Grant2024GX-YBXM-412; in part by the Fundamental Research Funds for the Central Universities, CHD under Grant 300102313208, Grant 300102314105, and Grant 300102314401.

Conflicts of Interest

The authors declare no conflicts of interest.

Ethical Approval and Consent to Participate

Not applicable.

References

[1] Wang, K., Zhang, J., Li, H., Wu, J., Wan, Q., Chen, T., ... & Luo, Y. (2024). Smart hydrogel sensors for health monitoring and early warning. *Advanced Sensor Research, 3*(9), 2400003. [CrossRef]

[2] Jin, Z., Zhao, F., Lei, Y., & Wang, Y. C. (2022). Hydrogel-based triboelectric devices for energy-harvesting and wearable sensing applications. *Nano Energy, 95*, 106988. [CrossRef]

[3] Pinaeva, U., Lairez, D., Oral, O., Faber, A., Clochard, M. C., Wade, T. L., ... & Soulé, A. (2019). Early warning sensors for monitoring mercury in water. *Journal of hazardous materials, 376*, 37-47. [CrossRef]

[4] Liu, D., Huyan, C., Wang, Z., Guo, Z., Zhang, X., Torun, H., ... & Chen, F. (2023). Conductive polymer based hydrogels and their application in wearable sensors: a review. *Materials Horizons, 10*(8), 2800-2823. [CrossRef]

[5] Sun, X., Agate, S., Salem, K. S., Lucia, L., & Pal, L. (2020). Hydrogel-based sensor networks: Compositions, properties, and applications—A review. *ACS Applied Bio Materials, 4*(1), 140-162. [CrossRef]

[6] Zhang, L., Han, C., Luo, W., Chen, X., Chen, X., & Yan, L. (2024). Curving-Stretching Induced Alignment in Hydrogel Actuators for Enhanced Grip Strength and Rapid Response. *ACS Applied Materials & Interfaces, 16*(41), 56126-56133. [CrossRef]

[7] Barhoum, A., Sadak, O., Ramirez, I. A., & Iverson, N. (2023). Stimuli-bioresponsive hydrogels as new generation materials for implantable, wearable, and disposable biosensors for medical diagnostics: Principles, opportunities, and challenges. *Advances in Colloid and Interface science, 317*, 102920. [CrossRef]

[8] Zhao, X., Chen, X., Yuk, H., Lin, S., Liu, X., & Parada, G. (2021). Soft materials by design: unconventional polymer networks give extreme properties. *Chemical Reviews, 121*(8), 4309-4372. [CrossRef]

[9] Montero de Espinosa, L., Meesorn, W., Moatsou, D., & Weder, C. (2017). Bioinspired polymer systems with stimuli-responsive mechanical properties. *Chemical reviews, 117*(20), 12851-12892. [CrossRef]

[10] Wu, J., Yun, Z., Song, W., Yu, T., Xue, W., Liu, Q., & Sun, X. (2024). Highly oriented hydrogels for tissue regeneration: design strategies, cellular mechanisms, and biomedical applications. *Theranostics, 14*(5), 1982. [CrossRef]

[11] Hang, C., Guo, Z., Li, K., Yao, J., Shi, H., Ge, R., ... & Xia, Y. (2025). Anisotropic hydrogel sensors with muscle-like structures based on high-absorbent alginate fibers. *Carbohydrate Polymers, 349*, 123015. [CrossRef]

[12] Zhang, R., Wang, W., Ge, Z., & Luo, C. (2025). Nonswellable and highly sensitive hydrogel for underwater sensing. *Journal of Polymer Research, 32*(1), 4. [CrossRef]

[13] Jiang, H., Jiang, S., Chen, G., & Lan, Y. (2024). Cartilage-inspired multidirectional strain sensor with high elasticity and anisotropy based on segmented embedded strategy. *Advanced Functional Materials, 34*(7), 2307313. [CrossRef]

[14] Wu, L., Kang, Y., Shi, X., Yuezhen, B., Qu, M., Li, J., & Wu, Z. S. (2023). Natural-wood-inspired ultrastrong anisotropic hybrid hydrogels targeting artificial tendons or ligaments. *ACS nano, 17*(14), 13522-13532. [CrossRef]

[15] Chen, Z., Wang, H., Cao, Y., Chen, Y., Akkus, O., Liu, H., & Cao, C. C. (2023). Bio-inspired anisotropic hydrogels and their applications in soft actuators and robots. *Matter, 6*(11), 3803-3837. [CrossRef]

[16] Wei, P., Chen, T., Chen, G., Hou, K., & Zhu, M. (2021). Ligament-inspired tough and anisotropic fibrous gel belt with programed shape deformations via dynamic stretching. *ACS applied materials & interfaces, 13*(16), 19291-19300. [CrossRef]

[17] Ye, S., Ma, W., & Fu, G. (2022). A novel nature-inspired anisotropic hydrogel with programmable shape deformations. *Chemical Engineering Journal, 450*, 137908. [CrossRef]

[18] Wang, S., Lei, L., Tian, Y., Ning, H., Hu, N., Wu, P., Jiang, H., Zhang, L., Luo, X., & Liu, F. (2024). Strong, tough and anisotropic bioinspired hydrogels. *Materials Horizons, 11*(9), 2131–2142. [CrossRef]

[19] Lin, H., Wang, R., Xu, S., Li, X., & Song, S. (2023).

Tendon-inspired anisotropic hydrogels with excellent mechanical properties for strain sensors. *Langmuir, 39*(17), 6069-6077. [CrossRef]

[20] Duan, S., Wu, S., Hua, M., Wu, D., Yan, Y., Zhu, X., & He, X. (2021). Tendon-inspired anti-freezing tough gels. *Iscience, 24*(9). [CrossRef]

[21] Luo, C., Huang, M., Sun, X., Wei, N., Shi, H., Li, H., ... & Sun, J. (2022). Super-strong, nonswellable, and biocompatible hydrogels inspired by human tendons. *ACS Applied Materials & Interfaces, 14*(2), 2638-2649. [CrossRef]

[22] Wang, Q., Zhang, Q., Wang, G., Wang, Y., Ren, X., & Gao, G. (2021). Muscle-inspired anisotropic hydrogel strain sensors. *ACS Applied Materials & Interfaces, 14*(1), 1921-1928. [CrossRef]

[23] Zhang, Y., Kou, K., Ji, T., Huang, Z., Zhang, S., Zhang, S., & Wu, G. (2019). Preparation of ionic liquid-coated graphene nanosheets/PTFE nanocomposite for stretchable, flexible conductor via a pre-stretch processing. *Nanomaterials, 10*(1), 40. [CrossRef]

[24] Lin, H., Yuan, W., Shao, H., Zhao, C., Zhang, W., Ma, S., ... & Song, S. (2024). Muscle-inspired anisotropic hydrogel strain sensors with ultra-strong mechanical properties and improved sensing capabilities for human motion detection and Morse code transmission. *European Polymer Journal, 202*, 112642. [CrossRef]

[25] Ghosh, A., Pandit, S., Kumar, S., Pradhan, D., & Das, R. K. (2024). Human muscle inspired anisotropic and dynamic metal ion-coordinated mechanically robust, stretchable and swelling-resistant hydrogels for underwater motion sensing and flexible supercapacitor application. *ACS Applied Materials & Interfaces, 16*(45), 62743-62761. [CrossRef]

[26] Kurhade, R. R., Shaikh, M. S., Nagulwar, V., & Kale, M. A. (2025). Advancements in carboxymethyl cellulose (CMC) modifications and their diverse biomedical applications: a comprehensive review. *International Journal of Polymeric Materials and Polymeric Biomaterials, 74*(11), 1043-1067. [CrossRef]

[27] Kang, J., & Yun, S. I. (2022). Double-network hydrogel films based on cellulose derivatives and K-carrageenan with enhanced mechanical strength and superabsorbent properties. *Gels, 9*(1), 20. [CrossRef]

[28] Wei, S., Qu, G., Luo, G., Huang, Y., Zhang, H., Zhou, X., ... & Kong, T. (2018). Scalable and automated fabrication of conductive tough-hydrogel microfibers with ultrastretchability, 3D printability, and stress sensitivity. *ACS Applied Materials & Interfaces, 10*(13), 11204-11212. [CrossRef]

[29] Park, N., & Kim, J. (2021). Anisotropic hydrogels with a multiscale hierarchical structure exhibiting high strength and toughness for mimicking tendons. *ACS Applied Materials & Interfaces, 14*(3), 4479–4489. [CrossRef]

[30] Liu, H., Wang, X., Cao, Y., Yang, Y., Yang, Y., Gao, Y., ... & Wu, D. (2020). Freezing-tolerant, highly sensitive strain and pressure sensors assembled from ionic conductive hydrogels with dynamic cross-links. *ACS Applied Materials & Interfaces, 12*(22), 25334-25344. [CrossRef]

[31] Aaryashree, Sahoo, S., Walke, P., Nayak, S. K., Rout, C. S., & Late, D. J. (2021). Recent developments in self-powered smart chemical sensors for wearable electronics. *Nano Research, 14*(11), 3669–3689. [CrossRef]

[32] Wang, X., Guo, C., Pi, M., Li, M., Yang, X., Lu, H., Cui, W., & Ran, R. (2022). Significant roles of ions in enhancing and functionalizing anisotropic hydrogels. *ACS Applied Materials & Interfaces, 14*(45), 51318–51328. [CrossRef]

[33] Chen, Z., Liu, J., Chen, Y., Zheng, X., Liu, H., & Li, H. (2020). Multiple-stimuli-responsive and cellulose conductive ionic hydrogel for smart wearable devices and thermal actuators. *ACS applied materials & interfaces, 13*(1), 1353-1366. [CrossRef]

[34] Han, S., Liu, C., Lin, X., Zheng, J., Wu, J., & Liu, C. (2020). Dual conductive network hydrogel for a highly conductive, self-healing, anti-freezing, and non-drying strain sensor. *ACS Applied Polymer Materials, 2*(2), 996-1005. [CrossRef]

[35] Chen, L., Chang, X., Chen, J., & Zhu, Y. (2022). Ultrastretchable, antifreezing, and high-performance strain sensor based on a muscle-inspired anisotropic conductive hydrogel for human motion monitoring and wireless transmission. *ACS applied materials & interfaces, 14*(38), 43833-43843. [CrossRef]

[36] Lin, F., Yang, W., Lu, B., Xu, Y., Chen, J., Zheng, X., ... & Huang, B. (2025). Muscle-Inspired Robust Anisotropic Cellulose Conductive Hydrogel for Multidirectional Strain Sensors and Implantable Bioelectronics. *Advanced Functional Materials, 35*(10), 2416419. [CrossRef]

[37] She, W., Shen, C., Xue, Z., Yu, J., Zhang, G., & Meng, Q. (2025). Constructing highly selective multidirectional hydrogel strain sensors with a pre-stretching strategy. *Journal of Materials Chemistry A*. [CrossRef]

[38] Li, L., Sun, Y., Ding, J., Wang, C., Xiang, Y., Guo, B., ... & Li, J. (2025). Gelatin-based anisotropic hydrogels for flexible sensors and bio-electrodes. *Chemical Engineering Journal, 519*, 164901. [CrossRef]

[39] Kong, W., Wang, C., Jia, C., Kuang, Y., Pastel, G., Chen, C., ... & Hu, L. (2018). Muscle-inspired highly anisotropic, strong, ion-conductive hydrogels. *Advanced Materials, 30*(39), 1801934. [CrossRef]

[40] Zhang, X., Crisci, R., Finlay, J. A., Cai, H., Clare, A. S., Chen, Z., & Silberstein, M. N. (2021). Enabling Tunable Hydrophilicity of PDMS via Metal-ligand Coordinated Dynamic Networks. [CrossRef]

[41] Jiang, H., Ou, C., Zhang, D., Hu, X., Ma, Y., Wang, M., ... & Xiao, L. (2023). Tough ion-conductive hydrogel

with anti-dehydration as a stretchable strain sensor for gesture recognition. *ACS Applied Polymer Materials, 5*(9), 6828-6841. [CrossRef]

[42] Zhong, L., Zhang, Y., Liu, F., Wang, L., Feng, Q., Chen, C., & Xu, Z. (2023). Muscle-inspired anisotropic carboxymethyl cellulose-based double-network conductive hydrogels for flexible strain sensors. *International Journal of Biological Macromolecules, 248*, 125973. [CrossRef]

[43] Liu, S., Wang, X., Peng, Y., Wang, Z., & Ran, R. (2021). Highly stretchable, strain-sensitive, and antifreezing macromolecular microsphere composite starch-based hydrogel. *Macromolecular Materials and Engineering, 306*(9), 2100198. [CrossRef]

[44] Sun, Y., Li, X., Zhao, M., Chen, Y., Xu, Y., Wang, K., ... & Zhang, X. (2022). Bioinspired supramolecular nanofiber hydrogel through self-assembly of biphenyl-tripeptide for tissue engineering. *Bioactive Materials, 8*, 396-408. [CrossRef]

[45] Chen, Z., Chen, X., Wang, H., Yang, T., Huang, J., & Guo, Z. (2025). Metal ion mediated conductive hydrogels with low hysteresis and high resilience. *Materials Today Physics, 51*, 101656. [CrossRef]

[46] Liu, Y., Jiang, D., Wu, Z., Jiang, B., & Xu, Q. (2024). Highly conductive and sensitive acrylamide-modified carboxymethyl cellulose/polyvinyl alcohol composite hydrogels for flexible sensors. *Sensors and Actuators A: Physical, 370*, 115258. [CrossRef]

[47] Choi, S., Fan, Z., Im, J., Nguyen, T. L., Park, N., Choi, Y., ... & Kim, J. (2025). Tendon-mimicking anisotropic alginate-based double-network composite hydrogels with enhanced mechanical properties and high impact absorption. *Carbohydrate Polymers, 352*, 123193. [CrossRef]

[48] Panda, P., Maity, P., Dutta, A., & Das, R. K. (2025). Anisotropic Anti-Swelling Hydrogels with Hydrophobic Association and Metal–Ligand Cross-Links for Applications in Underwater Strain Sensing and Anisotropic Actuation. *Langmuir, 41*(21), 13301-13314. [CrossRef]

[49] Zhang, S., Chen, X., Hu, Y., Shi, C., Li, Z., Bai, Z., & Zhou, Y. (2025). High-Strength Poly (vinyl alcohol) Hydrogels with Photo-and Metal-Ion-Induced Cross-Linking. *ACS Applied Polymer Materials, 7*(21), 14929-14941. [CrossRef]

[50] Wang, J., Li, X., & Liu, Y. (2025). Physically entangled hydrogels constructed through pre-stretched backbone provide excellent comprehensive mechanical properties. *Small, 21*(23), 2501666. [CrossRef]

[51] Zhang, X., Lang, B., Yu, W., Jia, L., Zhu, F., Xue, Y., ... & Zheng, Q. (2023). Magnetically induced anisotropic conductive hydrogels for multidimensional strain sensing and magnetothermal physiotherapy. *Chemical Engineering Journal, 474*, 145832. [CrossRef]

[52] Lv, X., Zhang, Q., Li, Z., Gong, K., Gao, B., Wei, H., & Li, P. (2025). Antifreezing, Water Retention, and High-Stretch Ionic Conductive Hydrogels for Winter Motion Sensing. *Journal of Applied Polymer Science*, e57130. [CrossRef]

[53] Li, Z., Chen, L., Liu, F., & Liu, X. (2025). Chitosan-based hydrogels with stretchable, self-healing, self-adhesive properties for flexible sensing applications. *Colloids and Surfaces A: Physicochemical and Engineering Aspects*, 138095. [CrossRef]

[54] Yu, W., Chen, J., Gao, Q., Guo, Y., Zhang, S., Pan, Y., ... & Wei, R. (2025). Multifunctional PVA/SA-based hydrogels integrating high stretchability, conductivity, and antibacterial activity for human-machine interactive flexible sensors. *Chemical Engineering Journal*, 164695. [CrossRef]

[55] Chen, C., Liu, P., Gu, Y., Pan, W., Liu, Y., Li, X., ... & Shan, X. (2025). Stretchable adhesive eutectic organohydrogel based on gelatin-Quaternized chitosan for wearable human motion monitoring. *International Journal of Biological Macromolecules*, 146939. [CrossRef]

[56] Jiang, H., Lai, J., Zhang, P., Lai, J., Tu, A., Lai, K., & Xiao, L. (2024). Low-Hysteresis Hydrogels with Antidehydration as a Stretchable Strain Sensor for Gesture Recognition. *ACS Applied Polymer Materials, 6*(19), 11922-11931. [CrossRef]

Appendix

A Experimental section

A.1 Characterization and Testing

The microstructures of P(DMAA-AA), P(DMAA-AA)-CMC, Zr^{4+}-P(DMAA-AA)-CMC, and zgel-X% hydrogels were characterized using FE-SEM (Hitachi S-4800). Samples were freeze-fractured in liquid nitrogen, lyophilized for 48 h, mounted on conductive tape, and sputter-coated with gold prior to imaging. Anisotropy was evaluated using POM (Leica DM4P) with cross-polarizers. Samples (zgel-X%, X = 0, 50, 100, 200) were rotated to $45°$, and birefringence images were captured using an integrated camera. Chemical structures were analyzed using an FTIR spectrometer (Nicolet iS 10) with ATR accessory. Spectra were recorded in the range of 4,000–650 cm^{-1} at a resolution of 4 cm^{-1}.

A.2 Swelling Ratio Tests

To evaluate the effects of metal ion crosslinking and pre-stretching on swelling behavior, swelling tests were conducted. Initially, hydrogel samples were freeze-dried for 48 h, and their dry weights (W_0) were recorded. The lyophilized samples were then

immersed in deionized water at room temperature (25°C) for 24 h to reach equilibrium swelling. After immersion, surface moisture was gently removed using filter paper, and the swollen weight (W_d) was measured. Each test was performed in triplicate to ensure statistical reliability. The swelling ratio (SR) was calculated as follows:

$$\text{Swelling ratio}(\%) = \frac{W_d - W_0}{W_0} \times 100\% \qquad \text{(A1)}$$

As shown in Equation A1, the swelling ratio quantifies the water absorption capacity of the hydrogels.

A.3 X-Ray Photoelectron Spectroscopy (XPS)

Surface elemental composition and chemical states of pristine and Zr^{4+}-crosslinked P(DMAA-AA)-CMC hydrogels were analyzed using XPS (Thermo K-Alpha). Spectra were acquired with a monochromatic Al Kα source (1486.6 eV), and binding energies were calibrated relative to the C 1s peak at 284.8 eV. Peak fitting and quantitative analysis were performed using Avantage software, referencing standard spectral libraries for accurate assignment of elemental states.

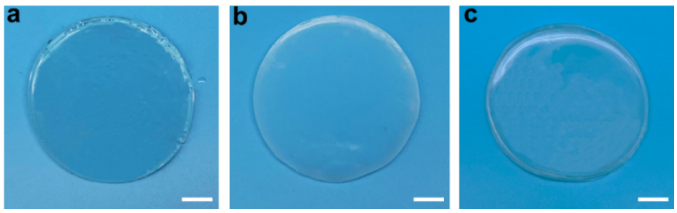


Figure A1. Photographs of (a) P(DMAA-AA), (b) P(DMAA-AA)-CMC, and (c) Zr^{4+}-P(DMAA-AA)-CMC hydrogels (scale bar: 1 cm).

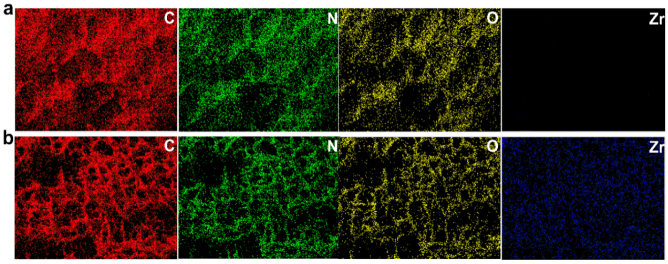


Figure A2. EDS spectra of P(DMAA-AA)-CMC and Zr^{4+}-P(DMAA-AA)-CMC hydrogels.

A.4 Contact Angle Measurements

Water contact angles were measured to assess surface wettability using a contact angle goniometer (OCA20, Dataphysics). A 4 μL droplet of deionized water was deposited onto flat, horizontal hydrogel surfaces via a microsyringe with programmable pump control.

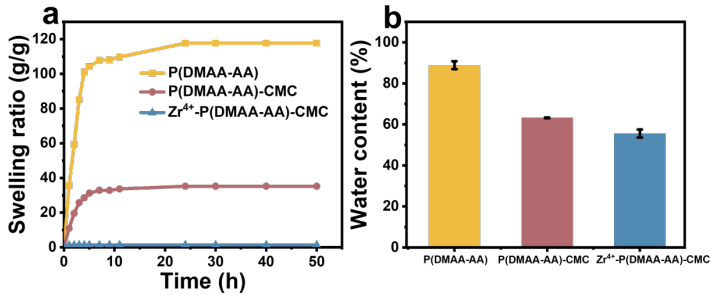


Figure A3. (a) Swelling ratio and (b) water content of P(DMAA-AA), P(DMAA-AA)-CMC, and Zr^{4+}-P(DMAA-AA)-CMC hydrogels.

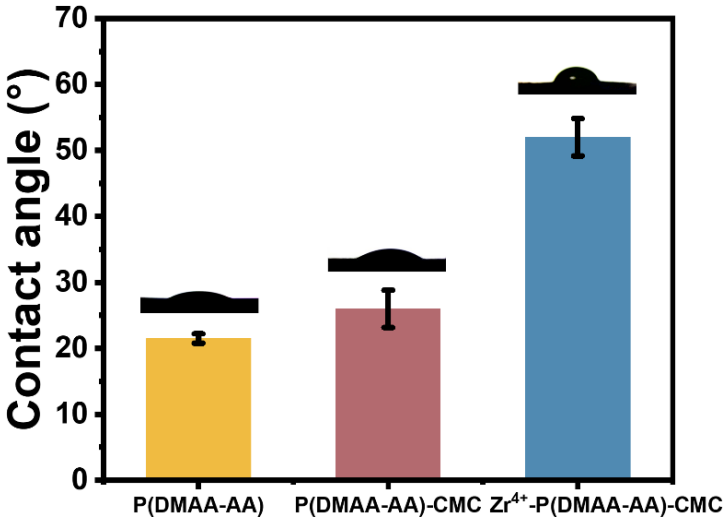


Figure A4. Water contact angles of P(DMAA-AA), P(DMAA-AA)-CMC, and Zr^{4+}-P(DMAA-AA)-CMC hydrogels.

Images of the stabilized droplet were captured within 5 s of deposition, and contact angles were analyzed using ImageJ software. Measurements were repeated at five different locations per sample to ensure consistency.

A.5 Mechanical Tensile Tests

Uniaxial tensile tests were performed using a universal testing machine (T-30, Shenzhen Sansi) equipped with a 100 N load cell. Hydrogel samples were cut into rectangular strips (10 mm × 40 mm × 2 mm) and tested at a strain rate of 50 mm/min. Stress (σ) and strain (ε) were calculated as:

$$\sigma = \frac{F}{A_0} \qquad \text{(A2)}$$

$$\varepsilon = \frac{L - L_0}{L_0} \times 100\% \qquad \text{(A3)}$$

where F is the applied load, A_0 is the initial cross-sectional area, L_0 is the initial gauge length, and L is the extended length. Stress-strain curves were analyzed via Origin software to determine tensile

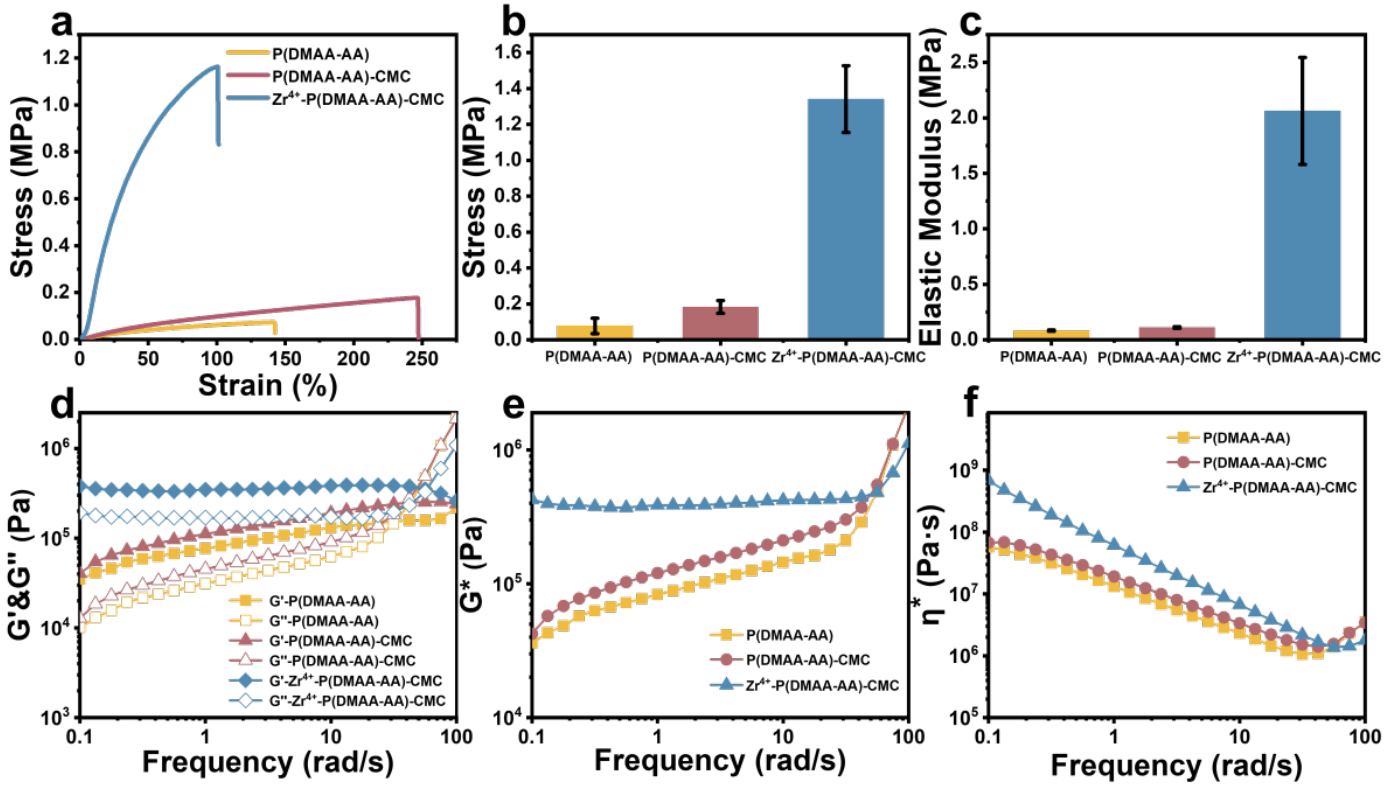


Figure A5. (a) Stress-strain curves, (b) stress plots, and (c) elastic modulus plots of P(DMAA-AA), P(DMAA-AA)-CMC, and Zr^{4+}-P(DMAA-AA)-CMC hydrogels; (d) oscillation frequency scan, (e) G^*, and (f) η^*.

Table A1. The comparation of anisotropy metrics.

Hydrogel	Tensile strength (MPa)	Strain coefficient (GF)	Ref.
alginate-based double-network composite hydrogels	5	/	[47]
Methacrylic acid-Fe^{3+} cross-linked anti-swelling hydrogel	2.7	/	[48]
High-Strength Poly(vinyl alcohol) Hydrogels	4.95	/	[49]
PAAm/PAAc Physically Entangled Hydrogels	0.33	/	[50]
anisotropic carboxymethyl cellulose-based double-network conductive hydrogels	4.32	/	[42]
Magnetically induced anisotropic conductive hydrogels	0.15	3.2	[51]
sodium alginate-co-polyacrylamide Ionic Conductive Hydrogels	1.67	2.58	[52]
Chitosan-based hydrogels	0.091	2.72	[53]
Multifunctional PVA/SA-based hydrogels	1.793	2.76	[54]
AM/Ge/QCS/CNFs/PBFDO-DES (AGQCP-DES) eutectic hydrogel	0.184	3.03	[55]
Low-Hysteresis Hydrogels with Antidehydration	0.18	2.6	[56]
Zr^{4+}-P(DMAA-AA)-CMC Pre-Stretching hydrogels	5.6	3.26	This work

strength, fracture strain, and elastic modulus. Three replicates were tested for each condition.

A.6 Rheological Characterization

Dynamic oscillatory shear tests were conducted using a rotational rheometer (MCR 302, Anton Paar) with 25 mm parallel plates. Frequency

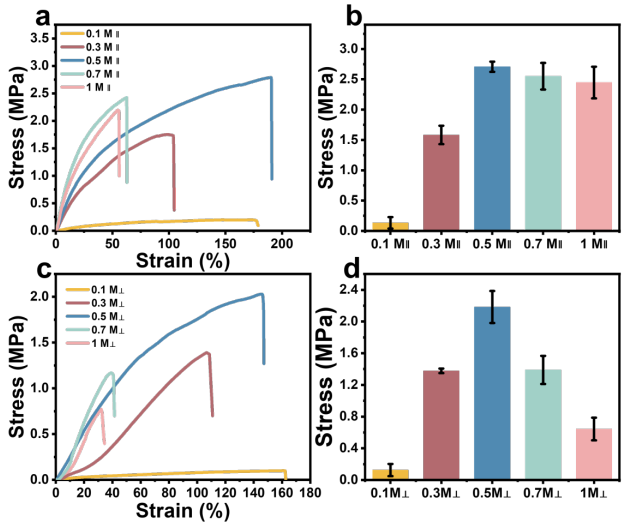


Figure A6. (a) Stress-strain curves and (b) stress plots of parallel-aligned zgel-100% hydrogels in Zr^{4+} solutions of varying concentrations; (c) stress-strain curves and (d) stress plots of perpendicular-aligned zgel-100% hydrogels in Zr^{4+} solutions of varying concentrations.

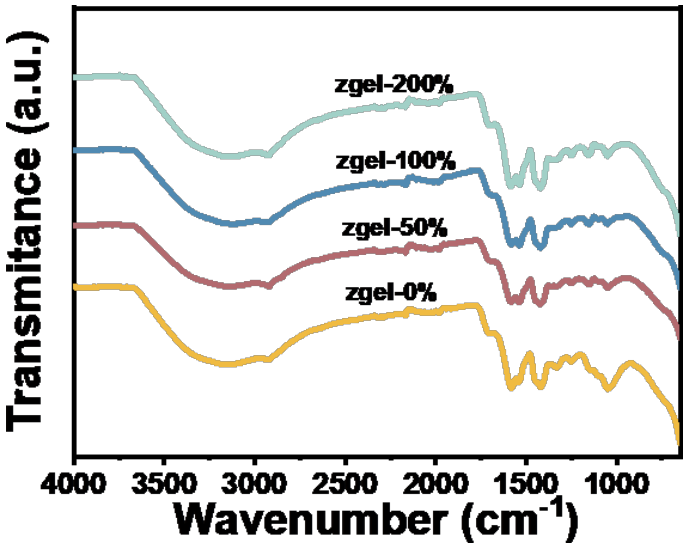


Figure A7. FTIR spectra of zgel-X% (X = 0, 50, 100, 200) hydrogels.

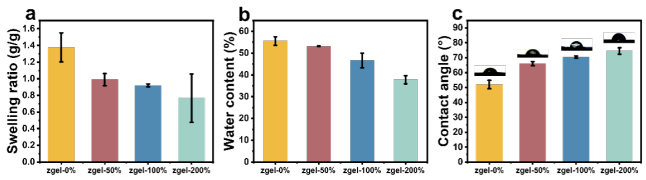


Figure A8. (a) Swelling ratio, (b) water content, and (c) water contact angle of zgel-X% (X = 0, 50, 100, 200) hydrogels.

sweeps (0.1–100 rad/s) were performed at 25°C to measure storage modulus (G′) and loss modulus (G″) for the following samples: P(DMAA-AA), P(DMAA-AA)-CMC, Zr^{4+}-P(DMAA-AA)-CMC, and

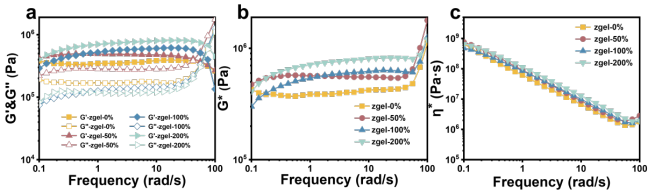


Figure A9. (a) Oscillation frequency scan, (b) G^*, and (c) η^* of zgel-X% (X = 0, 50, 100, 200) hydrogels.

zgel-X% (X = 50, 100, 200) hydrogels. Strain amplitude was maintained within the linear viscoelastic region (1% strain) to avoid structural disruption.

A.7 Tear Resistance Tests

Tear energy was evaluated via trouser tear tests using rectangular samples (40 mm length × 5 mm width × 0.5 mm thickness) with a 20 mm pre-cut notch. Samples were mounted on a universal testing machine (T-30) and stretched at 50 mm/min. Tear energy (Γ) was calculated as:

$$\text{Tear Energy} = \frac{1}{tL_{\text{bulk}}} \int F \, d\Delta \tag{A4}$$

where F is the force during tearing, Δ is displacement, t is sample thickness, and L_{bulk} is the residual length post-tearing.

A.8 Sensing Performance Evaluation

Real-time resistance changes during stretching were monitored using an electrochemical workstation (CHI660E, Shanghai Chenhua) coupled with the T30 tensile tester. Hydrogel sensors were stretched at controlled strains (0–100%) and strain rates (1–50 mm/min). Humidity was controlled at 50% using a humidifier to minimize environmental variability. Resistance (R) was calculated via Ohm's law:

$$R = \frac{U}{I} \tag{A5}$$

where U is the applied voltage and I is the measured current. Relative resistance change ($\Delta R/R_0$) and gauge factor (GF) were derived as:

$$\frac{\Delta R}{R_0} = \frac{R - R_0}{R_0} \tag{A6}$$

$$GF = \frac{\Delta R/R_0}{\varepsilon} \tag{A7}$$

where ε is the applied strain. A higher GF value indicates greater sensitivity to mechanical deformation, making the sensor suitable for high-precision strain detection applications.

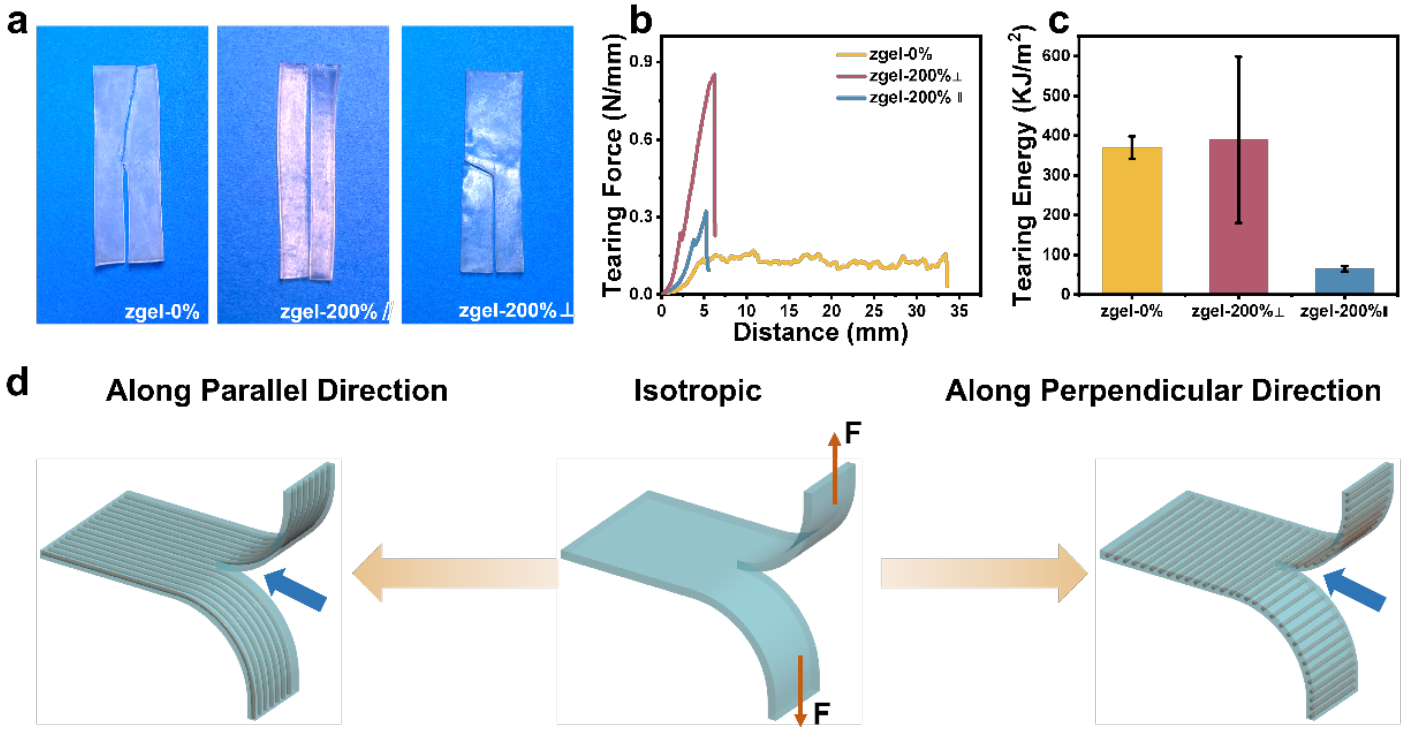


Figure A10. (a) Photographs of tear propagation along parallel and perpendicular directions of pre-stretched isotropic zgel-0% and anisotropic zgel-200% hydrogels; (b) force-displacement curves; (c) tear energy; (d) schematic of tear mechanism.

B Supplementary figures

The swelling capacity of the hydrogels is effectively tunable through compositional modification. As shown in Figure A3(a), P(DMAA-AA) exhibits the highest equilibrium swelling ratio (117.7 g/g), attributed to its macroporous structure that facilitates water infiltration and retention. In contrast, the incorporation of CMC significantly reduces swelling (35.2 g/g) due to enhanced hydrogen bonding, which tightens the polymer network and restricts water penetration. Further crosslinking with Zr^{4+} yields the lowest swelling ratio (1.37 g/g)-an 85-fold reduction compared to P(DMAA-AA)—resulting from additional chemical crosslinks that markedly limit water absorption.

Water content measurements (Figure A3(b)) corroborate this trend: P(DMAA-AA) shows the highest water content (88.8%), followed by P(DMAA-AA)-CMC (66.3%), and Zr^{4+}-crosslinked hydrogel (55.5%). The consistent decrease in both swelling ratio and water content, aligned with SEM observations, confirms that introducing CMC and Zr^{4+} progressively densifies the hydrogel network, providing a effective means to tailor its swelling behavior.

The surface wettability of the hydrogels was evaluated by contact angle measurements (Figure A4). P(DMAA-AA) exhibited the smallest contact angle (21.5°), indicating high hydrophilicity, which is consistent with its high swelling capacity. The introduction of CMC increased the contact angle to 26°, reflecting reduced surface hydrophilicity. In contrast, the Zr^{4+}-crosslinked hydrogel showed a markedly higher contact angle (over 52°), demonstrating enhanced hydrophobicity. This transition is attributed to the increased crosslinking density from Zr^{4+} ions, which reduces surface porosity and inhibits water adsorption [40, 41].

The mechanical properties of the hydrogels were systematically enhanced through the incorporation of CMC and Zr^{4+} cross-linking. Uniaxial tensile tests (Figure A5(a)) revealed that the pristine P(DMAA-AA) hydrogel exhibited low mechanical strength (stress: 73.2 kPa; strain: 115%). The addition of CMC significantly improved both stress (˜0.2 MPa) and strain (247%), owing to additional physical crosslinking via hydrogen bonds and electrostatic interactions [42]. Further reinforcement was achieved with Zr^{4+}, which raised the stress to 1.2 MPa—approximately 20 times that of P(DMAA-AA)—though with reduced strain

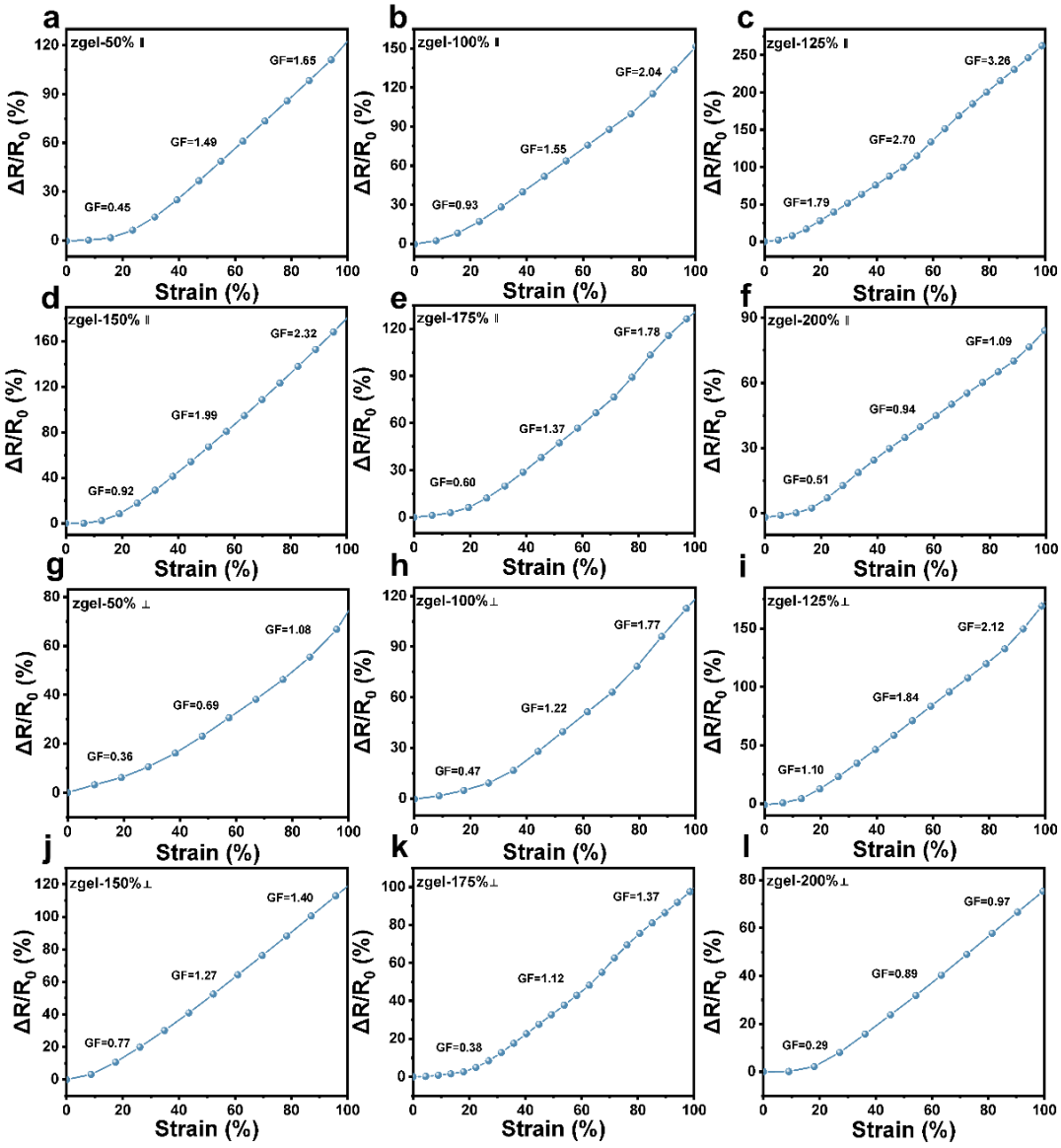


Figure A11. (a–f) Change in relative resistance versus strain for zgel-X% hydrogel strain sensors oriented parallel to the alignment direction; (g–l) Change in relative resistance versus strain for zgel-X% hydrogel strain sensors oriented perpendicular to the alignment direction.

(101%), indicating strengthened yet less extensible network formation. The elastic modulus of the Zr^{4+}-crosslinked hydrogel increased 25-fold to 2.1 MPa (Figure A5(c)), underscoring the pronounced effect of ionic crosslinking.

Rheological analysis confirmed these trends: all modified hydrogels showed solid-like behavior ($G' > G''$) across the tested frequency range (0.1–100 rad/s). The incorporation of CMC and Zr^{4+} led to a steady increase in complex modulus (G^*) and a decrease in complex viscosity (η^*), consistent with the formation of a more elastic and mechanically robust network [44].

The mechanical strength of the hydrogel exhibited a non-monotonic dependence on Zr^{4+} concentration, achieving optimal performance at 0.5 M. As shown in Figure A6(a, c), stress increased significantly with rising Zr^{4+} concentration up to 0.5 M, where parallel- and perpendicular-oriented samples reached stresses of 2.8 MPa and 2.0 MPa, respectively—representing 15- and 22-fold enhancements compared to the 0.1 M condition. Beyond this point, further concentration increases led to a decline in mechanical properties, with stresses dropping to approximately 2.2 MPa (parallel) and 0.8 MPa (perpendicular) at 1 M Zr^{4+}. This reduction, particularly the 46% decrease in perpendicular stress relative to the 0.5 M condition, indicates that excessive crosslinking disrupts network homogeneity and compromises tensile strength [45, 46]. Thus, while moderate Zr^{4+} concentrations

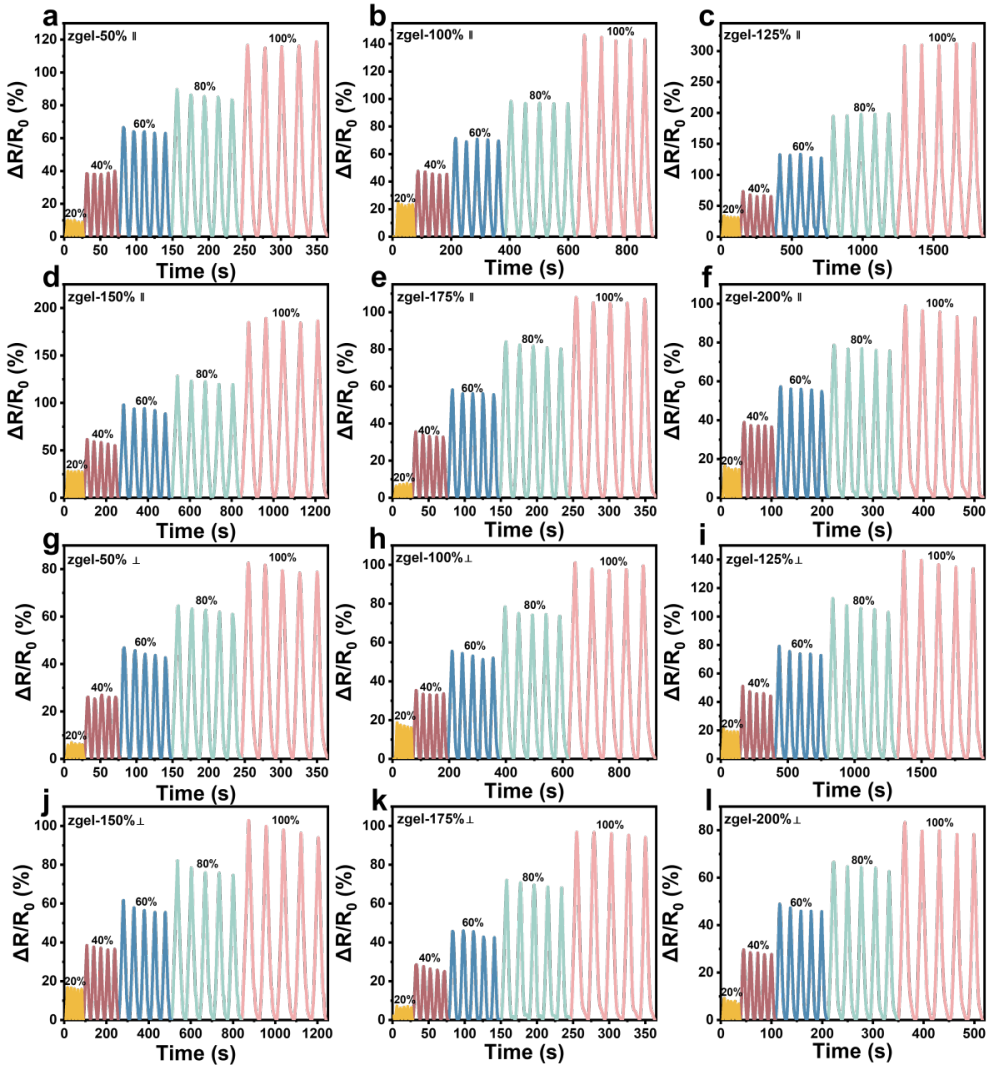


Figure A12. (a–f) Relative resistance changes of zgel-X% hydrogel strain sensors under different strains parallel to the orientation direction; (g–l) Relative resistance changes of zgel-X% hydrogel strain sensors under different strains perpendicular to the orientation direction.

significantly reinforce the hydrogel, surpassing a critical threshold leads to structural imbalance and mechanical deterioration.

FTIR analysis (Figure A7) confirms that pre-stretching induces only physical alignment of the hydrogel network without altering its chemical composition, as evidenced by unchanged characteristic peaks corresponding to O–H/N–H (3200–3500 cm^{-1}), C=O (1700 cm^{-1}), and C–O–C (1000–1200 cm^{-1}) bonds.

Increasing the pre-strain induces microstructural densification in the hydrogel, resulting in progressively lower swelling capacity (0.77 g/g at 200% strain), reduced water content (from 55.6% to 37.8%), and enhanced surface hydrophobicity (contact angle increase from 52° to 75°), as summarized in Figure A8(a–c).



Lixin Zhang is a master's candidate in the School of Materials Science and Engineering at Chang'an University, advised by Dr. Xi Chen and Professors Luke Yan. Her research focuses on the application of hydrogel materials in wound healing and biosensor fields. (Email: 983948953@qq.com)



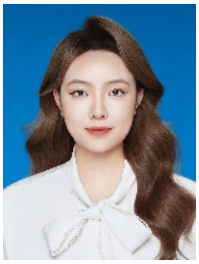
Zixuan Yang is a master's student at the School of Materials Science and Engineering, Chang'an University, and her supervisor is Dr. Chen Xi. Her research focuses on the performance exploration of oriented hydrogels. (Email: yzx2102852521@163.com)



Weihua Luo is currently an associate professor at the School of Materials Science and Engineering, Chang'an University. He earned his bachelor's degree from Wuhan University of Technology in 2000 and joined Chang'an University in the same year His research focuses primarily on materials science and mineralogy. (Email: weihual@chd.edu.cn)



Hongming Lu is a master's candidate in the School of Materials Science and Engineering at Chang'an University, advised by Dr. Xi Chen and Professor Luke Yan. Her research focuses on the application of hydrogel materials in wound healing. (Email: 2671044406@qq.com)



Ruiqi Zhao is a master's candidate at the School of Materials Science and Engineering, Chang'an University, under the supervision of Dr. Xi Chen and Professor Luke Yan. Her research focuses on the application of two-dimensional materials such as MXene and MBene, as well as hydrogel materials, in the field of photothermal evaporation. (Email: zhaorq1208@163.com)



Xi Chen is currently a faculty member at the School of Materials Science and Engineering, Chang'an University. He earned his Ph.D. from Tsinghua University in 2019. His research focuses on the preparation and biological applications of inorganic-organic hybrid nanofiltration membranes and hydrogels based on functional polymers. (Email: xi_chen@chd.edu.cn)



Xushuai Chen is a Ph.D. candidate in the School of Materials Science and Engineering at Chang'an University, under the supervision of Dr. Xi Chen and Professor Luke Yan. His research focused on the application of two-dimensional materials such as MXene, MOF materials, and hydrogels in the field of photothermal evaporation. (Email: 1319118134@qq.com)



Luke Yan is currently a professor at the School of Materials Science and Engineering, Chang'an University. His primary research interests include green and functional polymeric materials, green recycling and high-value utilization of waste plastics, novel polymeric membrane materials for wastewater treatment, and functional materials for transportation applications. (Email: lkyan@chd.edu.cn)